Time- and spectrally resolved terahertz photoconductivity of quantum Hall systems

C. Stellmach,[1] G. Vasile,[1] A. Hirsch,[1] R. Bonk,[1] Yu. B. Vasilyev,[2] G. Hein,[3] C. R. Becker,[4] and G. Nachtwei[1]
[1]*Institut für Angewandte Physik, Technische Universität Braunschweig, Mendelssohnstrasse 2, 38106 Braunschweig, Germany*
[2]*A.F. Ioffe Physical Technical Institute, Polytekhnicheskaya 26, 194021 St. Petersburg, Russia*
[3]*Physikalisch-Technische Bundesanstalt, Bundesallee 100, 38116 Braunschweig, Germany*
[4]*Physikalisches Institut, Universität Würzburg, Am Hubland, 97074 Würzburg, Germany*
(Received 26 April 2007; revised manuscript received 13 June 2007; published 31 July 2007)

We present terahertz photoconductivity measurements on GaAs/AlGaAs and HgTe/HgCdTe heterostructures. The photoresponse is investigated time and spectrally resolved under quantum Hall conditions. The samples are excited by a pulsed *p*-Ge laser, which emits photons of frequencies around 2 THz (corresponding to photon energies around 10 meV). Corbino-shaped GaAs/AlGaAs samples show relaxation times τ down to 10 ns. The dependence of τ on the applied source-drain voltage is explained by a two-level picture after normalizing the data. All spectrally resolved measurements show contributions of the cyclotron resonance and the bolometric effect. These results are compared to numerical calculations based on a self-consistent Born approximation method. The measurements on HgTe/HgCdTe samples show comparable results. However, the effective mass in these samples is only $m_c=0.026m_0$ (approximately 1/3 of the mass in GaAs/AlGaAs). Thus the cyclotron resonance is shifted to smaller magnetic fields around 2 T. This fact makes HgTe/HgCdTe systems especially interesting for terahertz detector applications.

DOI: 10.1103/PhysRevB.76.035341 PACS number(s): 73.43.Cd, 78.67.−n, 78.67.De, 07.57.Kp

I. INTRODUCTION

Quantum Hall (QH) systems[1,2] can be excited effectively by terahertz (THz) radiation, because the energy gap between the Landau levels and the photon energy are comparable (about 10 meV). The first investigations have been done more than 20 years ago,[3–5] most of the measurements are done on GaAs/AlGaAs samples patterned in Hall-bar or meander geometry. The investigations are interesting both with respect to basic questions about the excitation and relaxation processes of QH systems and with respect to application of these systems as high-performance THz detectors. It was shown[6–8] that QH detectors can reach a sensitivity up to 10^8 V/W and a relative detectivity of 10^{14} $\sqrt{\text{Hz}}$/W at 4.2 K, which are better than usual semiconductor bolometers working at the same temperature. In addition, QH detectors are fast and spectrally tunable.

In this paper, we discuss detailed time-resolved measurements of the photoconductivity on GaAs/AlGaAs QH samples in Corbino geometry. The system is excited by pulsed THz-laser radiation and the relaxation process is investigated. We find a dependence of the relaxation time on the applied source-drain voltage. The results are related to the Drude time and to the electron mobility. A normalized plot of the data is compared to the results of a two-level model of excitation and relaxation. Further, spectrally resolved measurements of the photoconductivity are presented. We compare this results with numerical calculations using a self-consistent Born approximation method. Finally, we introduce spectrally resolved and time-resolved measurements of the photoconductivity on HgTe/HgCdTe QH systems. This material system is promising for THz detector applications because of the possibility of operation at moderate magnetic fields ($B \leqslant 2$ T).

II. EXPERIMENTAL DETAILS

We use epitaxially grown GaAs/AlGaAs and HgTe/HgCdTe heterostructures, which provide a two dimensional electron gas (2DEG). Most of the experiments are performed on samples patterned in circular Corbino shape (inner and outer radii of the 2DEG are $r_1=500$ μm and $r_2=1500$ μm). All samples are characterized by Shubnikov–de Haas (SdH) measurements and by *I-V* curves. The sample properties are listed in Table I.

The samples were mounted in a He bath cryostat and operated at a temperature of 4 K. The sample magnetic field B is provided by a superconducting coil. We investigate the systems at high magnetic fields up to 7 T. A sketch of the setup is shown in Fig. 1.

The longitudinal conductivity σ_{xx} of a Corbino sample is proportional to the source-drain current I_{SD} at a source-drain voltage V_{SD}. For homogeneous systems, it is

$$\sigma_{xx} = \frac{I_{SD}}{V_{SD}} \frac{\ln(r_2/r_1)}{2\pi}.$$

In our setup, I_{SD} is measured by a voltage drop over a serial resistor [see Fig. 2(a)]. The photoresponse (PR) is the differ-

TABLE I. Sample properties: material, carrier concentration n_s, and mobility μ. The sample D_{Hall} is patterned in Hall-bar geometry; all other samples are patterned in Corbino geometry. The denoted mobilities in the case of Corbino samples are given by measurements at Hall-bar structures using the same wafer.

Sample No.	Material	n_s (m^{-2})	μ (m^2/V s)
A	GaAs/AlGaAs	2.7×10^{15}	10
B	GaAs/AlGaAs	2.0×10^{15}	50
C	GaAs/AlGaAs	1.9×10^{15}	150
D_{Hall}	HgTe/HgCdTe	3.8×10^{15}	4.1
E	HgTe/HgCdTe	4.4×10^{15}	4.1

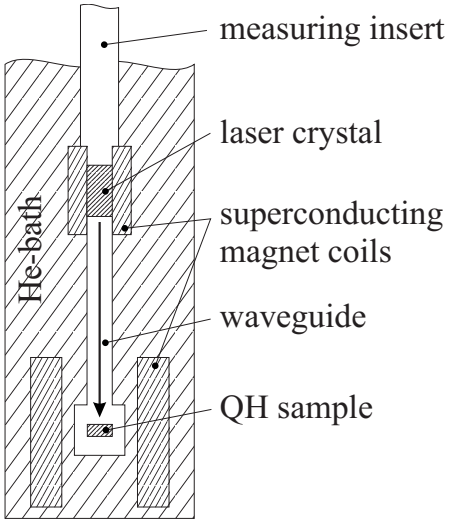

FIG. 1. Scheme of the measurement setup. The THz radiation is transfered via a 38 cm long waveguide from the laser crystal to the QH sample.

ence of the signal measured with and without illumination: PR $\propto \Delta I_{SD} \propto \Delta \sigma_{xx}$. For the time-resolved measurements, the signal is transferred via a 50-Ω-terminated coaxial line. The *RC* time of the circuit is less than 10 ns.

The THz radiation is generated by a *p*-Ge laser, which is operated in pulsed mode. The laser crystal has a hole concentration of $p \approx 10^{19}$ m^{-3}. Strong magnetic and electric fields are necessary for the operation of the laser. The magnetic field of around 3 T is provided by an additional superconducting coil. Since the laser is based on the cyclotron resonance of light holes in Ge, the photon frequency is controlled by the magnetic field. Our laser is tunable from 1.7 to 2.5 THz (corresponding to wavelengths of 180–120 μm). The linewidth of a *p*-Ge laser is as low as 6 GHz.[9]

The electric field for the laser is generated by applying a high voltage to the laser crystal. This voltage is generated by a high power pulse generator (voltage about 1–2 kV; current about 15–20 A). For the time-resolved measurements, we constructed a special fast switching pulse generator with a switch-off time of $\leqslant$20 ns (see Ref. 10 for details).

The laser system and the QH sample are mounted in the same cryostat. The THz radiation is transmitted via a brass waveguide onto the sample. The setup is shown schematically in Fig. 1.

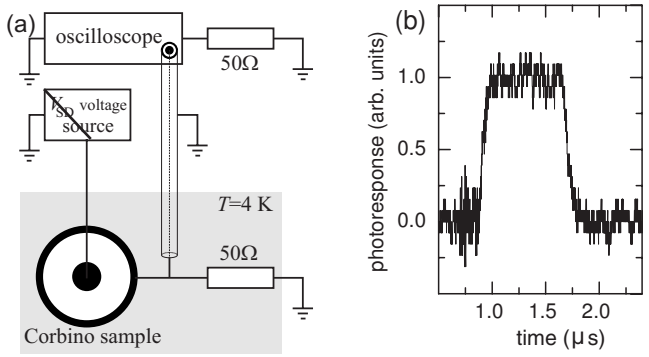

FIG. 2. (a): Circuit with impedance matched signal line. (b) A typical shape of the time-resolved PR during one laser pulse.

III. TIME-RESOLVED MEASUREMENTS

The time-resolved measurements of the PR are done with the setup shown in Fig. 2(a). The QH sample is exposed to pulsed THz radiation. To suppress the effect of electromagnetic cross-talking between the cables, two measurements are taken: with and without applied voltage V_{SD} on the QH sample (see Ref. 11 for more details about this method).

A typical shape of the time-resolved PR is shown in Fig. 2(b). The laser pulse causes an optically induced breakdown of the QH effect, yielding a sharp increase of the PR during this process. After this we observe a constant PR. Finally, the PR decreases after the radiation is switched off, because the system relaxes back into the QH state.

To characterize the time of the relaxation process, we apply an exponential function of the form

$$\mathrm{PR} \propto \exp(-t/\tau), \tag{1}$$

with the decay time τ and the time t. This is done in detail for the GaAs/AlGaAs samples at filling factor $\nu=2$. To compare the data to a more complex function than Eq. (1) is not possible because of the limited measuring resolution (on meander shaped samples, showing time scales in the millisecond and microsecond ranges, a more complex behavior was identified in the past[7,12]).

We find decay times τ from about 10 to over 200 ns (this is by several orders of magnitude shorter than the time scales found on meander type detectors[8,12]). There is the trend that τ increases with increasing mobility of the sample μ. Further, there is a particular dependence of τ on the voltage V_{SD}. This fact proves that the results are due to time scales inside the QH system and are not dominated by influences of our setup.

For the two low mobility samples A and B, we find conspicuous maxima slightly below the QH breakdown voltages V_c. To compare the results obtained at samples with different electron mobilities, the curves are plotted versus normalized axes in Fig. 3. The voltage is divided by V_c (voltage of electrical QH breakdown), which is a characteristic voltage of the system. The decay time is divided by τ_{Drude}, which corresponds to the mobility μ according to $\tau_{\mathrm{Drude}}=\mu m^*/e$ (with the electron charge e and the effective mass m^*) and is a characteristic time of the system. We see in this scale a quite similar behavior of samples A and B, with a good match of the maxima near $V_{SD}/V_c=1$ (sample C shows a different behavior; this will be discussed later). We explain this result with a heating picture as follows.

We consider the relaxation from a dissipative state back to the QH state when the THz radiation is switched off. This relaxation process of hot electrons is comparable to the situation reported in Ref. 13, where a spatially resolved process is discussed. Like those authors, let us assume a two-level model and a signal, which is proportional to occupation N of the upper level: PR $\propto N$. The occupation of the upper level decreases by a certain rate, but is increased by Joule heating, which is proportional to V_{SD}^2 and to j^2 (where j is the current

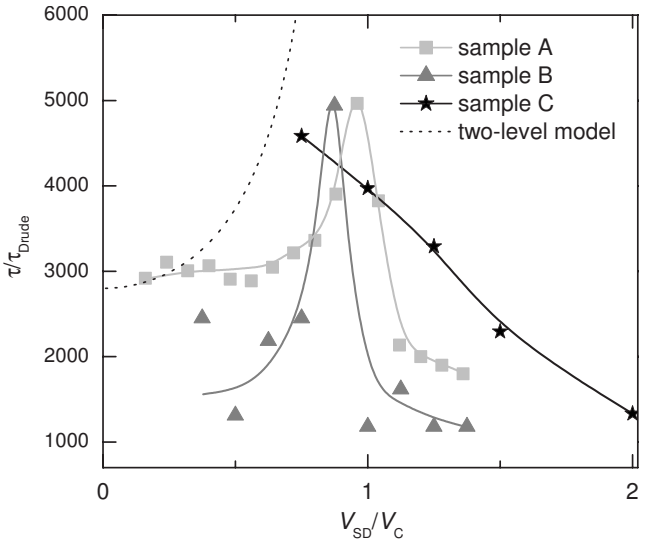

FIG. 3. The decay time for the GaAs/AlGaAs samples plotted versus normalized axes. The decay time is divided by the Drude time and the applied voltage is divided by the QH breakdown voltage.

density inside the Corbino disk). Therefore a high current prevents a fast relaxation of the hot (optically generated) electrons. This behavior may explain the results shown in Fig. 3 (for $V_{SD}<V_c$; for $V_{SD}>V_c$, there is no QH state any more, but there is a transition between dissipative states, which is fast). The process is described by the rate equation[13,14]

$$dN = dN_{gain} - dN_{loss} = \frac{\rho_{xx} j^2}{\hbar \omega_c} dt - N\frac{dt}{\tau_0}, \tag{2}$$

where $\hbar\omega_c$ is the cyclotron engery. From this follows

$$\mathrm{PR} \propto N \propto e^{-(t/\tau_0)[1-(j/j_c)^2]}. \tag{3}$$

Comparing this with Eq. (1), one finds

$$\tau = \tau_0 \frac{1}{1-\left(\frac{j}{j_c}\right)^2} = \tau_0 \frac{1}{1-\left(\frac{V_{SD}}{V_c}\right)^2}. \tag{4}$$

The function $\tau(V_{SD})$ approaches τ_0 at $V_{SD}=0$ and increases for $V_{SD}\to V_c$, as shown in Fig. 3. This reproduces partially the experimental results.

For source-drain voltages near V_c and above, the system cannot reach the QH state and the measured decay time τ describes the change between dissipative states. This concerns a different kind of relaxation time. One can say that, for $V_{SD}\geqslant V_c$, the relaxation process *to the QH state* takes an infinitely long time. This corresponds to the divergence of the function (4) at $V_{SD}=V_c$.

Sample C with the highest mobility shows a different behavior. We see no decrease of τ for $V_{SD}\to 0$ (for $V_{SD}/V_c < 0.75$, no reliable data could be measured, because of the low signals for small V_{SD}). In Ref. 13, the sample with the highest mobility (104 $m^2/V\,s$) also differs from the behavior of the remaining samples. This was attributed to a longer spatial range of potential fluctuations at higher mobilities. This is conceivable also in our case.

IV. SPECTRALLY RESOLVED MEASUREMENTS

In the spectrally resolved measurements, the PR is measured versus the magnetic field B. This is done for the GaAs/AlGaAs samples for different conditions. The PR signal is measured during the laser pulse, when the optically excited system is in a stationary equilibrium (the PR is not influenced by the switching processes of the laser).

Figure 4(a) shows the PR around the filling factor $\nu=2$ for sample B (medium mobility) measured with different photon energies for three different voltages V_{SD}. For $V_{SD}=2$ and 3 V, the system can reach the QH state and plateaus are visible in the transport curves. For $V_{SD}=5$ V, the breakdown voltage V_c is exceeded. The highest PR is observed near the integer filling factor for all voltages. In case of the QH plateaus, the PR shows typically two peaks correlated to the left and right flanks of the plateau (double-peak structure). For $V_{SD}=5$ V, there is one peak bound to the SdH minimum. This signal, called bolometric PR, is due to heating of the 2DEG by the THz radiation, yielding a change of the conductivity (see, for example, Refs. [4–6] and Sec. V).

On the other hand, additional peaks are visible at magnetic fields where the system is in cyclotron resonance (CR), according to

$$E_{ph} = \hbar\omega_c = \hbar eB/m^*, \tag{5}$$

where E_{ph} is the photon energy. (Our measurements yield $m^*=0.067m_0$, which is in good agreement with other studies.[15,16]) In some cases, the CR peaks are negative [see Fig. 4(a), $V_{SD}=2$ V, $B>5$ T]. We attribute this behavior as follows. The conductivity of QH systems decreases with increasing temperature for filling factors distinctively outside the QH plateau. As the negative CR peaks shown in Fig. 4(a) occur just for these noninteger filling factors, this results in a negative photoresponse. For $E_{ph}\leqslant 8.1$ meV, the CR peaks overlap strongly with the bolometric effect. Both effects add to each other, yielding highest PR.

A different type of measurement is shown in Fig. 4(b), where the photon energy is fixed, but the electron concentration is tuned by a gate voltage V_G, yielding a shift of the QH plateau. In this case, the overlap of bolometric and CR effects can be controlled by V_G because the maximal bolometric signal is bound to the QH plateau.

We observe the superposition of the bolometric and CR effects in all our measurements and find that it depends on different parameters, for example, on the electron mobility μ of the system. The results for sample A (low mobility) are shown in Fig. 5. The PR is measured for different laser photon energies and two different voltages V_{SD}. For both voltages, clear bolometric peaks, bound to the flanks of the plateau, are observed. The position of the laser line E_{ph} influences the shape of the bolometric peaks: The highest signal appears when the laser line is positioned at a flank of the plateau. Single CR peaks are not directly resolvable. To recognize the influence of E_{ph} more clearly, we plot the data

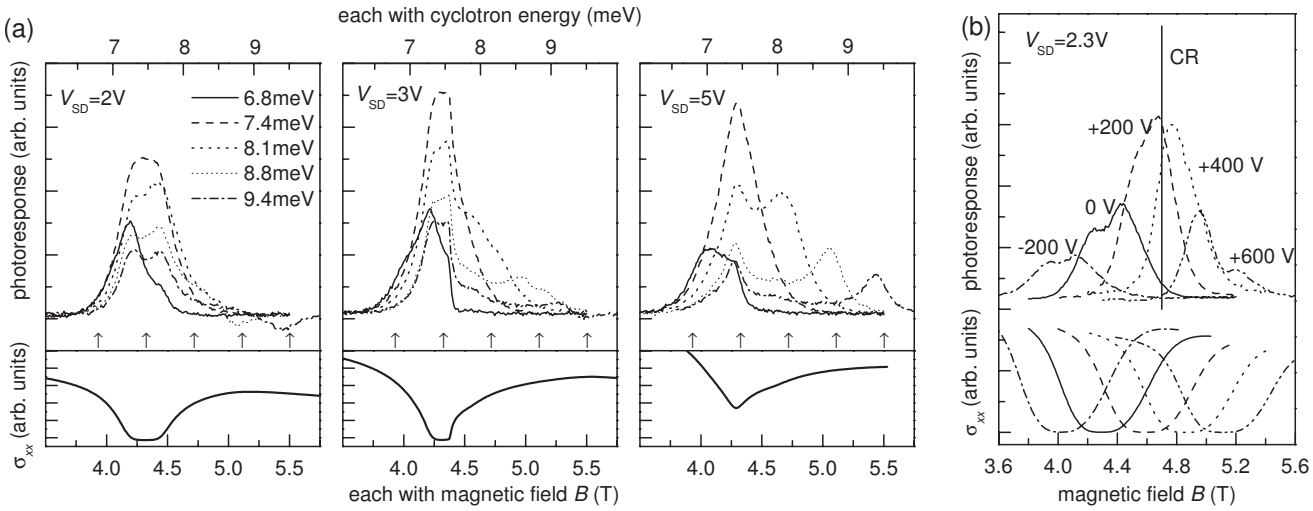

FIG. 4. The photoresponse of sample B versus the magnetic field. (a) The photoresponse is measured at three different voltages V_{SD}, each with five different photon energies E_{ph}. The photon energies are noted in the legend and marked by arrows. At this positions, cyclotron resonance peaks in the photoresponse are visible. In the lower part of the figures, σ_{xx} is plotted versus the magnetic field. (b) The laser photon energy is fixed at 8.1 meV and the photoresponse is measured for five different carrier concentrations (gate voltages are marked). In the lower part of the figure, σ_{xx} is plotted versus the magnetic field.

in a different way: In Fig. 5(b), the PR is plotted versus the magnetic field $B \propto \omega_c$ and the the photon energy E_{ph}. The gray tones correspond to the PR magnitude. We see an enhanced PR in the region corresponding to the QH plateau and along the CR line ($E_{ph}=\hbar\omega_c$). The maximal PR is found at $E_{ph} \approx 9$ meV and $B \approx 5.4$ T, where the bolometric and CR effects overlap.

QH systems are promising candidates for high-performance and tunable THz detectors. For this application, the system is spectrally tuned by the magnetic field to vary the cyclotron energy $\hbar\omega_c$. To reach a maximum of the PR, the carrier concentration must be adjusted accordingly, too. An important parameter for detector applications is the spectral resolution. To determine this value, we plotted the PR measured at a fixed E_{ph} for different cyclotron energies and adjusted n_s. Figure 6 shows the result for sample B [the data are taken from Fig. 4(b)]. The data can be modeled by a Lorentzian function. The maximum appears in good agreement with the expected value $E_{ph}=\hbar\omega_c$. The spectral resolution corresponds to the full width at half maximum, yielding $\Gamma \approx 1$ meV (corresponding to $\Gamma/E_{ph} \approx 0.12$). This is the best

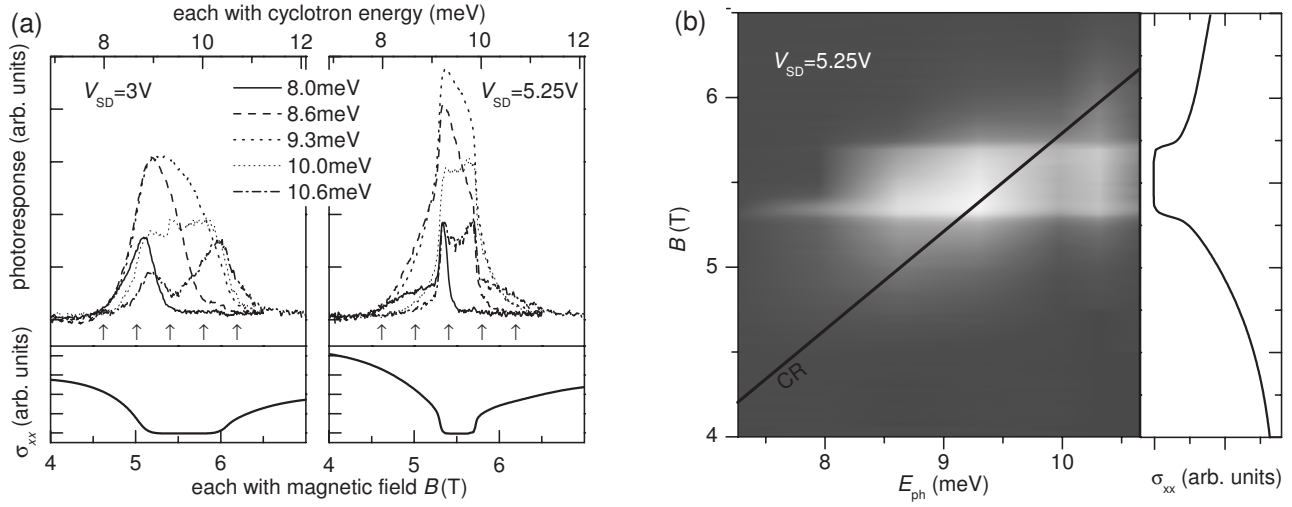

FIG. 5. (a) Photoresponse of sample A versus the magnetic field, displayed like in Fig. 4(a). The photoresponse is measured for two different voltages V_{SD}. (b) The PR plotted versus the photon energy and the magnetic field for sample A. The gray tones correspond to the PR magnitude (light ≙ high PR). Furthermore, in the right part, the σ_{xx} curve is shown for orientation. The PR is enhanced in the magnetic field region of the plateau (bar of enhanced PR from $B=5.3$ to 5.7 T). In addition, a calculated line corresponding to the CR condition (5) is drawn in. Along this line, there is an enhanced PR, too (at least near the plateau region.) The highest PR is found at the crossing of the CR line, and the plateau region. This figure shows the CR part of the PR more conspicuously than (a) (same data).

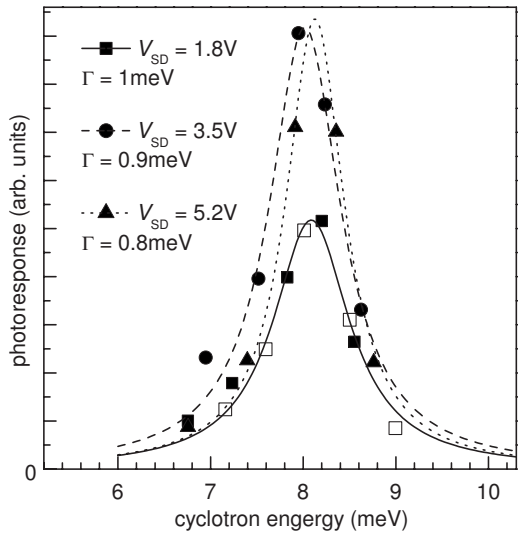

FIG. 6. The spectral resolution of sample B. The photon energy of the laser is fixed to 8.13 meV. The data points are taken from the PR measured versus the cyclotron energy E_c for three different voltages V_{SD} (the carrier concentration is adjusted accordingly). For V_{SD}=1.8 V, the PR is plotted at the left and right flanks of the second QH plateau, respectively. To estimate the spectral resolution, a Lorentzian fit in the form $\Gamma/[4(\hbar\omega_c - E_{ph})^2 + \Gamma^2]$, with the full width at half maximum Γ, is performed.

value we obtained. Other samples in this study show broader distributions.

V. NUMERICAL CALCULATIONS

The experimental results show clearly that the PR is affected by two main mechanisms: the CR and bolometric effects. Under CR conditions, the system can efficiently absorb radiation. This yields a heating of the electron system and a resulting change of the conductivity (bolometric effect). An enhanced PR is observed near the QH plateaus, in particular, at the flanks of the plateaus, because there the heat capacity is small and the conductivity changes enormously with the temperature.

For a theoretical treatment, we consider the dynamic conductivity of the system. Classically, the dynamic conductivity can be calculated by solving the Drude equation of motion. We perform a quantum mechanical calculation by using a self-consistent Born approximation (SCBA).[17] Figure 7 shows the real part of the conductivity $\mathrm{Re}(\sigma_{xx}(\omega))$ as a result (here, $\omega = E_{ph}/\hbar$ is the photon frequency). This example is calculated for a damping parameter $\gamma_B^2 = 2e/(\pi^2\hbar n_s \mu) = 0.01$ (corresponding to wafer A). The highest values of $\mathrm{Re}(\sigma_{xx}(\omega))$ are found roughly near along the CR line. Further structures are due to Landau quantization. For $\omega = 0$, the static conductivity is reproduced, which shows minima at even-numbered filling factors (note that $\hbar\omega_c/E_F = 2/\nu$, E_F is the Fermi energy and spin splitting is not taken into account).

The absorption A and the absorbed power P_{in} are proportional to $\mathrm{Re}(\sigma_{xx}(\omega))$:

$$P_{in} \propto A \propto \mathrm{Re}(\sigma_{xx}(\omega)). \tag{6}$$

The absorption leads to an increase of the temperature of the 2DEG. The temperature increase ΔT, in addition, depends on

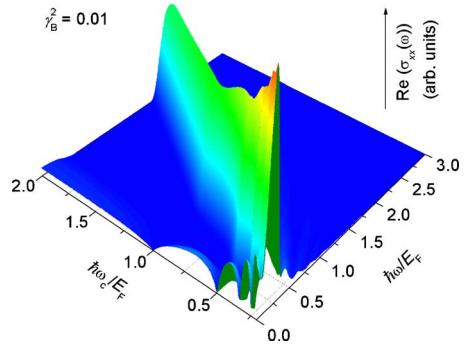

FIG. 7. (Color online) Real part of the dynamic conductivity, plotted versus the cyclotron and photon energies, numerically calculated by the SCBA method.

different parameters such as the heat coupling and the heat capacity of the 2DEG and the exposure time.

The heat capacity c can be calculated from the density of states, given by the SCBA:

$$c = \left[\frac{\partial(\text{inner energy})}{\partial T}\right]_{n_s} \tag{7a}$$

$$= \int (E - \mu_{ch}) Z(E) \left[\frac{\partial}{\partial T} f(E, \mu_{ch}, T)\right]_{n_s} dE. \tag{7b}$$

Here, f is the Fermi function and μ_{ch} the chemical potential. Figure 8(a) shows c plotted versus the filling factor. The calculation yields a minimum of c at even-numbered filling factors for a low temperature. In contrast, typically at higher temperatures, a narrow maximum and two minima nearby are found at even-numbered filling factors (see, for example, the solid curve at $\nu = 2 \Leftrightarrow \hbar\omega_c/E_F = 1$). This behavior is confirmed qualitatively by the results of Zawadzki and Lassing[18] and Gornik *et al.*[19]

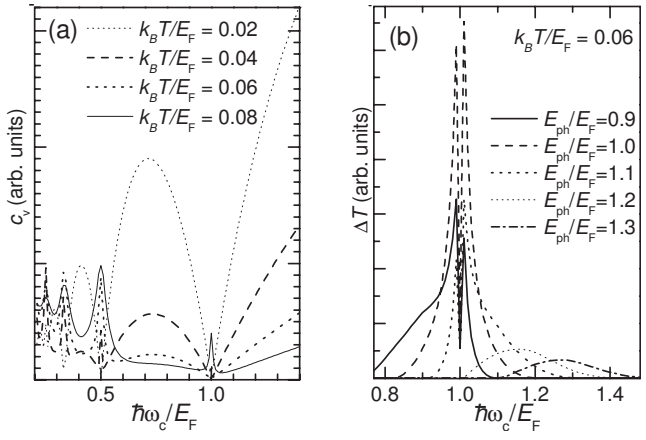

FIG. 8. Calculated results for a damping parameter $\gamma_B^2 = 0.0023$. (a) Heat capacity for different temperatures ($k_BT/E_F = 0.06$ corresponds to $T \approx 5$ K). (b) Calculated change of the temperature for different photon energies E_{ph} according to Eq. (8).

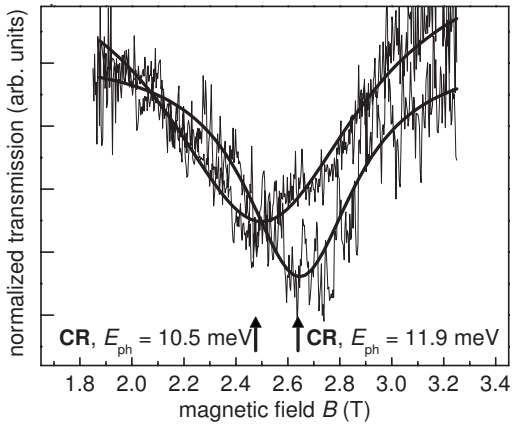

FIG. 9. Normalized THz transmission (Voigt configuration) of wafer E at two different photon energies plotted as a function of the magnetic field. A p-Ge crystal was used as a detector. The CR peaks are fitted by Lorentzian functions.

If c is taken as an essential parameter, the change of the temperature can be calculated as follows:

$$\Delta T \propto \frac{P_{\text{in}}}{c} \propto \frac{\text{Re}(\sigma_{xx}(\omega))}{c}. \tag{8}$$

The result of this procedure is shown in Fig. 8(b) with dependence on the filling factor for different photon energies E_{ph} and γ_B^2=0.0023 (corresponding to wafer B).

As expected, ΔT has maxima at $\omega=\omega_c$ (CR) and double peaks close to $\nu=2$. The latter appear due to the special structure of $c(\hbar\omega_c/E_F)$. The result is comparable to the experimental curves as shown in Figs. 4(a), V_{SD}=3 and 5 V.

VI. PHOTORESPONSE OF HgTe/CdHgTe SAMPLES

The investigations of the THz PR of devices with HgTe quantum wells embedded in Cd-HgTe barriers were aimed at obtaining photosignals at smaller magnetic fields. The quantum wells have a thickness of 12 nm, so that they possess a semimetallic band structure.[20] We found an effective mass of about m_c=0.026m_0 for our samples from transmission cyclotron resonance measurements. The results are shown in Fig. 9. As this cyclotron mass is by almost a factor of 3 smaller than that of electrons in GaAs, the same Landau level splitting as in GaAs is reached at about 1/3 of the magnetic field. It should be noted that the band structure of this material is nonparabolic. The nonparabolicity has various consequences. One is the dependence of the cyclotron mass m_c on the carrier density n_s. The higher n_s is, the higher is m_c. Thus, the value for m_c as measured by CR experiments on our samples is determined by n_s of the samples investigated in this study.

In Fig. 10, the PR of sample D_{Hall} is shown for three laser energies. Here, the PR is shown as a function of the magnetic field B. In the B range of the fourth QH plateau (near $B \approx 4.1$ T), we find two distinct maxima of the PR. Since the laser is emitting photons with an energy well below the CR condition, this effect is due to bolometric heating of the system by the THz radiation. The PR signal is by about a factor

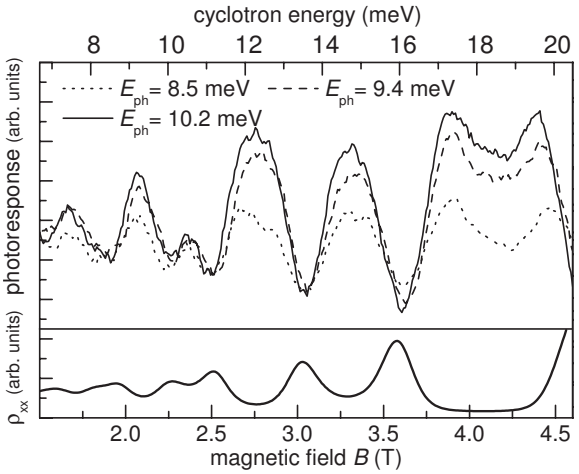

FIG. 10. Photoresponse of the sample D_{Hall} versus the magnetic field for different laser photon energies in the upper part of the figure. The transport curve is shown in the lower part.

of 10 smaller than in comparable GaAs/AlGaAs samples. However, also the HgTe/HgCdTe samples show a spectral selectivity even in their bolometric signal. This is visible in Fig. 11 for sample E. A variation of the laser energy leads to a change of the amplitude of the PR. In Fig. 12, this spectral resolution of this Corbino-shaped sample is presented as PR versus the photon energy. The position of the CR is marked by an arrow. As visible, the measured data are asymmetric with respect to the maximum. The asymmetry is possibly due to the strong nonparabolicity of the band structure of the material.[20] Taking the spectral resolution Γ from this curve, one obtains $\Gamma/E_{\text{ph}} \approx 0.6$ (it is $\Gamma \approx 4.6$ meV). This resolution is not as good as for GaAs/AlGaAs samples. However, the HgTe/HgCdTe samples show also a spectral resolution in their bolometric PR.

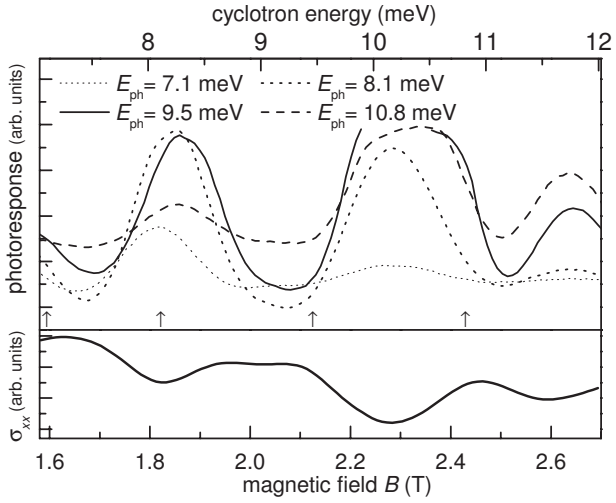

FIG. 11. Photoresponse of sample E versus the magnetic field for different laser photon energies in the upper part of the figure. The transport curve is shown in the lower part. Photon energies are marked by arrows. (The solid curve is interrupted, because such a high PR was reached, that the preset measurement range was overshot.)

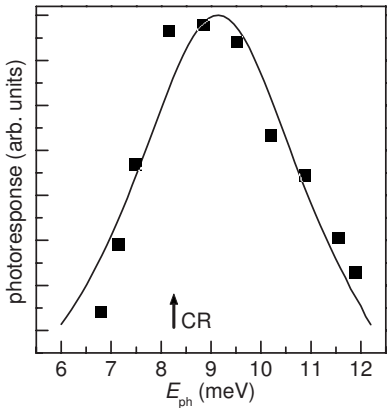

FIG. 12. Spectral resolution of sample E. The photoresponse is plotted versus the photon energy at $B=1.55$ T. The data points are fitted by a Lorentzian function. The CR position is marked.

Further, we measured the relaxation time of optically excited carriers in sample E. Similar to the GaAs samples, the system is excited by short laser pulses. The photoresponse of HgTe/HgCdTe samples is rather weak. Therefore the disturbances caused by electromagnetic coupling of the setup appear relatively strong in the result. Thus, a precise determination of intrinsic switching times is not possible. An estimation yields $\tau < 100$ ns.

Thus, the HgTe/HgCdTe samples are also suitable for the spectrally resolved and fast observation of THz radiation. Although these samples are less sensitive and possess a spectral resolution less pronounced as for GaAs-based samples, the HgTe/HgCdTe samples can be operated at lower magnetic fields ($B \leqslant 2$ T).

VII. SUMMARY

The subject of this work is the experimental investigation of the terahertz photoconductivity in systems under quantum Hall conditions. The investigations are interesting with respect to possible applications of quantum Hall systems as high-performance terahertz detectors. On the other hand, basic questions about the photoconductivity of QH systems are addressed. As a terahertz source, a *p*-Ge laser system was used, which emits a radiation of a frequency around 2 THz, corresponding to a photon energy of about 10 meV. The measurements were performed on GaAs/AlGaAs and HgTe/HgCdTe heterostructures at a low temperature $T=4$ K and high magnetic fields up to 7 T.

We performed detailed time-resolved measurements of the PR of the GaAs/AlGaAs samples. In particular, the relaxation of the system after the switching off of the illumination was investigated. We found relaxation times τ from 10 ns to over 200 ns, depending on the source-drain voltage V_{SD} and the electron mobility μ. These time scales are by orders of magnitude shorter than results of Hall-bar and meander samples published before. For comparison, we plot our results on a normalized scale (τ divided by the Drude time and V_{SD} divided by V_c). In this scale, the samples with $\mu \leqslant 50$ m^2/V s are very similar. We discuss our result by a two-level model, which treats the stationary equilibrium between excitation and relaxation processes.

In addition, we discuss spectrally resolved measurements of the GaAs/AlGaAs samples. The photosignal is explained by a superposition of cyclotron resonance and a bolometric effect. The spectral resolution Γ was determined by measurements of the photoresponse as a function of the magnetic field. The best value of about $\Gamma=1$ meV at $E_{ph} \approx 8$ meV is reached by a sample with Corbino geometry and with an electron mobility of 50 m^2/V s. The typical interaction of cyclotron resonance and a bolometric effect is analyzed by numerical calculations. The calculations are based on a self-consistent Born approximation method and can reproduce qualitatively the experimental results.

Finally, some investigations are performed on HgTe/HgCdTe systems. To our knowledge, on these systems, no terahertz photoconductivity measurements have been published by other groups yet. Because of the low effective mass, the CR appears at moderate magnetic fields (around 2 T at 9 meV). Because of the possibility of operation at moderate magnetic fields, this material system is especially interesting for detector applications, for which quantum Hall systems are promising because of their high sensitivity, spectral tunability, and fast response.

ACKNOWLEDGMENTS

This work was supported by the Deutsche Forschungsgemeinschaft DFG-Schwerpunktprogramm "Quanten-Hall-Systeme," Project No. NA235/10-2/3. The authors thank R. R. Gerhardts for supporting the calculations. The investigated wafers were provided by the MBE groups of the Max-Plank Institut für Festkörperforschung, Stuttgart, Germany, and the Universität Würzburg, Germany.

[1] K. v. Klitzing, G. Dorda, and M. Pepper, Phys. Rev. Lett. **45**, 494 (1980).

[2] K. von Klitzing, Rev. Mod. Phys. **58**, 519 (1986).

[3] J. C. Maan, T. Englert, D. C. Tsui, and A. C. Gossard, Appl. Phys. Lett. **40**, 609 (1982).

[4] D. Stein, G. Ebert, K. von Klitzing, and G. Weimann, Surf. Sci. **142**, 406 (1984).

[5] R. E. Horstmann, E. J. v. d. Broeck, J. Wolter, R. W. van der Heijden, G. L. J. A. Rikken, P. M. F. H. Sigg, J. Maluenda, and J. Hallais, Solid State Commun. **50**, 753 (1984).

[6] K. Hirakawa, K. Yamanaka, M. Endo, M. Saeki, and S. Komiyama, Phys. Rev. B **63**, 085320 (2001).

[7] Y. Kawano, Y. Hisanaga, H. Takenouchi, and S. Komiyama, J. Appl. Phys. **89**, 4037 (2001).

[8] Y. Kawaguchi, K. Hirakawa, M. Saeki, K. Yamanaka, and S. Komiyama, Appl. Phys. Lett. **80**, 136 (2002).

[9] Opt. Quantum Electron. **23**, 111 (1991), special issue on FIR semiconductor lasers, edited by E. Gornik and A. A. Andronov.
[10] C. Stellmach, Ph.D. thesis, Technische Universität Braunschweig, 2007.
[11] C. Stellmach, A. Hirsch, G. Nachtwei, Y. B. Vasilyev, N. G. Kalugin, and G. Hein, Appl. Phys. Lett. **87**, 133504 (2005).
[12] N. G. Kalugin, Y. B. Vasilyev, S. D. Suchalkin, G. Nachtwei, B. E. Sağol, and K. Eberl, Phys. Rev. B **66**, 085308 (2002).
[13] I. I. Kaya, G. Nachtwei, K. von Klitzing, and K. Eberl, Phys. Rev. B **58**, R7536 (1998).
[14] K. Güven, R. R. Gerhardts, I. I. Kaya, B. E. Sağol, and G. Nachtwei, Phys. Rev. B **65**, 155316 (2002).
[15] F. Thiele, U. Merkt, J. P. Kotthaus, G. Lommer, F. Malcher, U. Rössler, and G. Weimann, Solid State Commun. **62**, 841 (1987).
[16] B. A. Andreev, I. V. Erofeeva, V. I. Gavrilenko, A. L. Korotkov, A. N. Yablonskiy, O. Astafiev, Y. Kawano, and S. Komiyama, Semicond. Sci. Technol. **16**, 300 (2001).
[17] T. Ando, J. Phys. Soc. Jpn. **38**, 989 (1975).
[18] W. Zawadzki and R. Lassnig, Surf. Sci. **142**, 225 (1984).
[19] E. Gornik, R. Lassnig, G. Strasser, H. L. Störmer, A. C. Gossard, and W. Wiegmann, Phys. Rev. Lett. **54**, 1820 (1985).
[20] A. Pfeuffer-Jeschke, Ph.D. thesis, Universität Würzburg, 2000.